IEEE Control Systems Letters paper presented at
2023 American Control Conference (ACC)
San Diego, CA, USA. May 31 - June 2, 2023

Energy amplification of stochastically-forced hypersonic blunt body flows

Anubhav Dwivedi and Mihailo R. Jovanović

Abstract— **We utilize stochastically-forced compressible linearized Navier-Stokes equations to study the dynamics of hypersonic flows over blunt bodies. Our analysis of the energy of the flow fluctuations around the laminar stagnated flow reveals strong amplification of specific streamwise and spanwise length scales. We also provide insights into how changes in different physical parameters, such as the temperature of the blunt body and its curvature, influence the amplification of flow fluctuations. We show that increasing the bluntness and decreasing the wall temperature can significantly enhance the amplification of flow fluctuations. Our approach offers a systematic control-theoretic framework for quantifying the influence of stochastic excitation sources (e.g., free-stream turbulence and surface roughness) that are unavoidable in experiments and paves the way for the development of control-oriented models of hypersonic flows over blunt bodies.**

I. Introduction

Vehicle surface heating at hypersonic flow conditions, where the fluid flows at least five times faster than the speed of sound, is a major concern: an unmanaged thermal loading on vehicle surface can lead to structural failure. Throughout the flight geometry, the largest amount of heating typically appears at the nose tip of the flight vehicle, where the high-speed flow undergoes a rapid deceleration as it interacts with the solid surface for the first time [1]. A common approach to reduce this heat flux is to increase the bluntness by decreasing the curvature of the nose-tip [2]. However, experiments in wind-tunnels indicate that such an increase in the bluntness causes an early transition from a laminar to turbulent flow [3], [4] which introduces an additional source of aerodynamic heating: surface temperatures are about five times larger in turbulent than in laminar flow [5]. The dynamics at such extreme flow conditions are poorly understood, especially in the presence of uncertainties that are typical in experimental setups and flight configurations. The development of control-oriented models that can account for the robustness of laminar flows at hypersonic conditions is critically important for vehicle performance and survivability. In this paper, we analyze the dynamical properties of the blunt body flow in the presence of spatially distributed and temporally varying external disturbances.

The early onset of flow transition in the blunt body flows at hypersonic conditions has been a subject of numerous experimental [6], [7] and numerical investigations [8], [9]. The classical approach to understanding transition onset involves carrying out a spectral (i.e. normal mode) analysis of the linearized compressible flow equations. In this framework, if given flow conditions lead to unstable normal modes then the linearized dynamical generator associated with the laminar flow is also unstable. However, previous applications of the hydrodynamic stability analysis [10] indicate that the blunt body flow is stable. Furthermore, as the radius of the nose-tip increases, the flow is found to become more stable, which is in contrast to the experimental observations that indicate an early onset of flow transition with an increase in bluntness [4], [7]. Recently, it has been recognized that even in asymptotically stable flows, transient (finite-time) growth can play significant role [11], [12] in the transition process. This approach has been utilized to identify the 'worst case' initial state in the blunt body flows [13], [14] that can lead to the largest energy growth of flow fluctuations. However, these initial states may not be realizable in experiments. In this context, we adopt a complementary viewpoint by utilizing an input-output approach. This framework allows us to quantify the influence of modeling imperfections which are unavoidable in physical systems, thereby bringing in an appealing robustness interpretation.

A major source of uncertainty in the wind-tunnel experiments appears in the form of free-stream turbulence which is often unavoidable at hypersonic flow conditions [15], [16]. The presence of turbulence introduces a source of unsteady stochastic excitation whose detailed modeling often requires very expensive numerical computations [17]. In the present work, we utilize an input-output framework that models the influence of turbulence as small amplitude white-in-time external disturbances. These disturbances are considered as inputs, while various combinations of velocities and temperature are considered as outputs.

Input-output (I/O) analysis that evaluates the response (outputs) of the linearized Navier-Stokes (NS) equations to external perturbation sources (inputs) has been successfully employed to quantify the amplification and study transition mechanisms in low speed channels [18]–[20], boundary layers [21]–[23], jets [24] and hypersonic shock-boundary-layer-interactions [25]–[28]. In this paper, we utilize the I/O analysis to demonstrate that the hypersonic blunt bodies strongly amplify external stochastic excitations with a specific spanwise and streamwise length scale. Furthermore, our analysis also indicates that in the presence of background noise, increasing the bluntness and decreasing wall temperature can cause a dramatic increase in disturbance amplification which agree well with experimentally observed trends.

Financial support from the Air Force Office of Scientific Research (under award FA9550-18-1-0422) and the Office of Naval Research (under award N00014-19-1-2037) is gratefully acknowledged.

Anubhav Dwivedi and Mihailo R. Jovanović are with the Ming Hsieh Department of Electrical and Computer Engineering, University of Southern California, Los Angeles, CA 90089, USA. Emails: dwivedia@usc.edu and mihailo@usc.edu

Our presentation is organized as follows. In § II, we introduce hypersonic blunt body flow. In § III, we provide linearized model associated with the blunt body flow and a brief summary of the input-output formulation. In § IV, we evaluate the energy amplification in the presence of background noise and quantify the role of physical parameters such as nose-bluntness and wall temperature on the robustness of the laminar hypersonic flow. We conclude our presentation in § V.

II. Laminar stagnation point flow

To analyze the response of hypersonic blunt body flows to small external disturbances, we first evaluate the mean flow near the stagnation point. Throughout our presentation, we assume calorically perfect gases.

First, we provide a brief physical description of the flow near the stagnation region. Figure 1 (a) shows a canonical flow over a planar blunt body obtained from a numerical simulation [29]. Most significant heat transfer into the vehicle surface appears at the leading edge, where the free-stream hypersonic flow undergoes a rapid deceleration before stagnation. To obtain the steady flow in this region, consider the zoomed-in view in figure 1 (b). The high-speed flow prior to stagnation is characterized by large value of Mach number $M := U_\infty/c_\infty$, where U_∞ is the free-stream velocity and c_∞ is the free-stream speed of sound. This corresponds to the $M \gg 1$ flow in region-1. After the shock wave, the flow in region-2 is considerably slower, i.e. $M \ll 1$, and the flow turns begins to turn as we move closer to the wall (see the streamtraces which are locally aligned with the flow velocity). However, very close to the wall, the viscous effects become important, and a stagnation boundary layer starts to develop as shown in figure 1 (c). Next, we describe our methodology for obtaining the flow after the shock.

1) Inviscid flow in region-2: The flow conditions in region-1 are specified in terms of the state $\mathbf{q}_1 = (\rho_1, u_1, T_1)$, which denotes the density, the $x-$component of velocity, and the temperature, respectively. Furthermore, $\mathbf{q}_1$ is assumed to be independent of the spatial coordinates in this region. Across the shock, near the stagnation point, the state of the gas is given by $\mathbf{q}_2 = (\rho_2, u_{2w}, T_2)$, where u_{2w} denotes the velocity along the surface, i.e., along the direction x_w (see figure 1(b) for reference). Abusing notation, we will drop the subscript w from u_{2w}. To obtain $\mathbf{q}_2$ we utilize conservation of mass, momentum and energy across a normal shock wave,

$$\begin{aligned}
\rho_2 &= \rho_1 \frac{(\gamma+1)M^2}{2+(\gamma-1)M^2}, \\
u_2 &= \frac{2\Delta x_w}{\mathcal{R}} \sqrt{\frac{(\gamma M^2+1)\rho_1 R T_1}{(\gamma+1)\rho_2}}, \\
T_2 &= T_1 \left(\frac{2\gamma}{\gamma+1}M^2 - \frac{\gamma-1}{\gamma+1}\right)\left(\frac{2}{(\gamma+1)M^2} + \frac{\gamma-1}{\gamma+1}\right),
\end{aligned} \tag{1}$$

where $\mathcal{R}$ denotes the nose-tip radius of the blunt body (see figure 1), $\gamma = 1.4$, R denotes the gas constant, and Δx_w is the distance along the surface with the stagnation point as the origin. Note that the flow close to the stagnation location, i.e. when $\Delta x_w \ll 1$, is considerably slower than the free-stream flow in the region-1. The radius $\mathcal{R}$ is the key parameter which determines how quickly the flow accelerates in the region-2: larger bluntness leads to smaller velocity gradients. After determining $\mathbf{q}_2$ from equation (1), we can obtain the viscous flow close to the wall as described below.

2) Boundary layer flow in region-3: The state in region-3 close to the wall is given by $\mathbf{q}_3 = (\rho_3, u_3, T_3)$, where u_3 denotes the velocity along the surface, i.e., along the direction x_w. Unlike regions-1 and 2, determining $\mathbf{q}_3$, in general, requires solving boundary layer equations which are a set of coupled parabolic partial differential equations (PDEs) [1]. However, close to the stagnation region, these PDEs can be simplified using the Lees-Dorodnitsyn transformations by changing the coordinates (x_w, y_w) to (ξ, η) through,

$$\begin{aligned}
\xi(x_w) &:= \int_0^{x_w} \rho_2 u_2 \mu_2 \,\mathrm{d}x, \\
\eta(x_w, y_w) &:= \frac{u_2}{\sqrt{2\xi}} \int_0^{y_w} \rho \,\mathrm{d}y.
\end{aligned} \tag{2}$$

As shown in figure 1 (c), the stagnation boundary layer develops slowly in the x_w direction. The introduction of transformations in equation (2), allows us to look for similarity solutions [1],

$$f' = f'(\eta) = \frac{u_3}{u_2}, \quad g = g(\eta) = \frac{T_3}{T_2}. \tag{3}$$

In other words, even though $\mathbf{q}_3$ varies along the coordinates (x_w, y_w), it is only a function of η in the transformed coordinates. As a result, the non-dimensional stagnation boundary layer equations can be expressed as coupled ordinary differential equations (ODEs),

$$\begin{aligned}
(Cf'')' + ff'' &= (f')^2 - g, \\
\left(\frac{C}{Pr}g'\right)' + fg' &= 0,
\end{aligned} \tag{4}$$

where, Pr denotes the Prandtl number of the gas. In general, the variable C also depends on the properties of the gas and the pressure variation along the blunt body. However, for the present work, we assume that the gas of interest is air with constant $Pr \approx 0.72$. Furthermore, the pressure across the stagnation point can be well approximated as constant which allows us to express $C = g^{-0.28}$ and $\rho_3 = \rho_2 T_2/T_3$. The ODEs in the equation (4) are accompanied by the following boundary conditions,

$$\begin{aligned}
&\text{at } \eta = 0 \,(\text{wall}),\ f = f' = 0; g = g_w, \\
&\text{at } \eta \to \infty \,(\text{region-2}),\ f' = 1; g = 1,
\end{aligned} \tag{5}$$

where $g_w := T_w/T_2$ is the ratio of wall temperature to the temperature in the region-2. Physically, the values of the boundary condition $g_w \in (0, 1]$. For example, $g_w = 1$ implies a surface which is in thermal equilibrium with the stagnated flow, while $g_w < 1$ signifies a surface which is cooler than the surrounding fluid. Equation (5) illustrates that the value of g_w together with the nose-tip radius $\mathcal{R}$ serve as the two

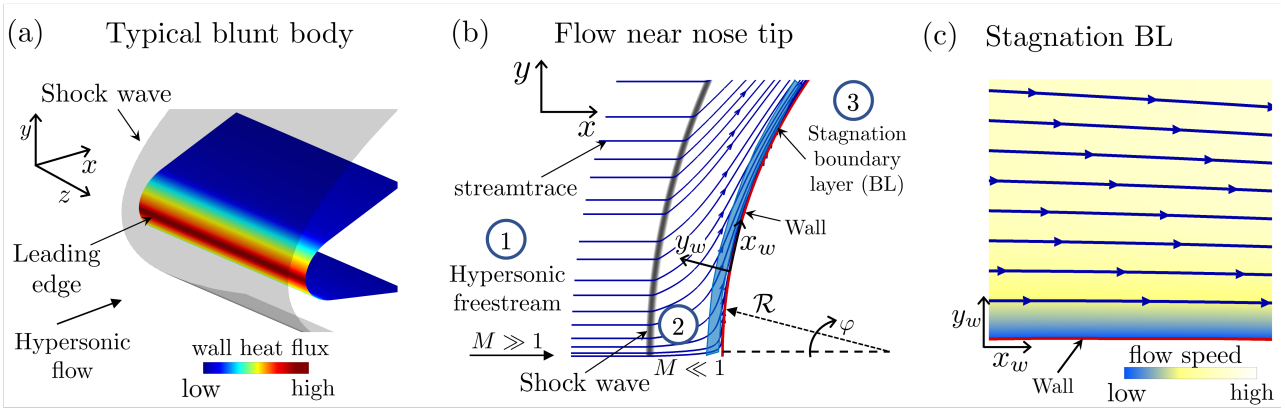

Fig. 1. (a) The spatial variation of the heat flux into a typical blunt body at hypersonic conditions; (b) zoomed in view near the nose tip; (c) stagnation boundary layer in region-3.

parameters in the blunt-body flow.

Past experiments on blunt bodies often observe a rapid transition of laminar boundary layer to a turbulent one. The experimental observations indicate that the transition process moves closer to the stagnation region as the $\mathcal{R}$ decreases or if the wall temperature g_w is reduced [4], [7]. This observation is in contrast with the classical linear hydrodynamic theory which does not identify any exponentially growing modes. However, the classical approach does not account for the role of uncertainties encountered in flight or in ground experiments at hypersonic conditions. In the rest of this work, we will examine the response of the stagnation point flow to external excitations.

III. Externally Forced Linearized Compressible Equations: Input-Output Framework

In this section, we examine the linearized dynamics of fluctuations associated with the blunt-body flow in the presence of external disturbances. A large amplification of the flow fluctuations can lead to a rapid transition of the mean flow from a laminar to turbulent state.

The mean flow in the present case is assumed to be the flow in the regions-2 and 3. As illustrated in the previous section, this base state only depends on η (the boundary layer coordinate). Transforming back to the (x_w, y_w, z) coordinates, the quantities ρ, U, T are constant in the $z-$coordinate but they vary slowly with the surface aligned x_w-direction [1]. In this work we assume that this variation along x_w is negligible, allowing us to simplify our analysis through Fourier transform. The linearized equations are

$$\begin{aligned}
\frac{\partial u}{\partial t} + \mathrm{i}k_x U u &= -vU' + \frac{1}{\bar{\rho} Re_l}\zeta_x,\\
\frac{\partial v}{\partial t} + \mathrm{i}k_x U v &= \frac{1}{\bar{\rho} Re_l}\zeta_y,\\
\frac{\partial w}{\partial t} + \mathrm{i}k_x U w &= \frac{1}{\bar{\rho} Re_l}\zeta_z,\\
\frac{\partial \theta}{\partial t} + \mathrm{i}k_x U \theta &= -vT' - (\gamma-1)T(\nabla\cdot\mathbf{u})\\
&\quad + \frac{\gamma}{\rho \,\mathrm{Pr}\, Re_l}\Theta,
\end{aligned} \tag{6}$$

where

$$\begin{aligned}
\zeta_x &= \mathrm{i}k_x(\lambda\nabla\cdot\mathbf{u} + 2\mathrm{i}k_x\mu u + 2\mu' T' U'\theta)\\
&\quad + (\mu'(u' + \mathrm{i}k_x v) + (\mu' T' U')'\theta) +\\
&\quad + (\mu(u'' + \mathrm{i}k_x v') + \mu' T' U'\theta') +\\
&\quad - k_z\mu(k_z u + k_x w) + \mathrm{i}k_z \frac{d\mu}{dT} U_1'\theta\\
\zeta_y &= \mathrm{i}k_z(\mu(\mathrm{i}k_x v + u') + \mu' T' U_1'\theta)\\
&\quad + (\lambda'\nabla\cdot\mathbf{u} + 2\mu' v') + (\lambda(\nabla\cdot\mathbf{u})' + 2\mu v'')\\
&\quad + \mathrm{i}k_z(\mu(\mathrm{i}k_z v + w'))\\
\zeta_z &= -\mu\left(k_x^2 w + k_z k_x u\right) + \mathrm{i}k_x\mu' T' U'\theta +\\
&\quad (\mu(w' + \mathrm{i}k_z v))' + \mathrm{i}k_z(\lambda\nabla\cdot\mathbf{u} + 2\mathrm{i}k_z\mu w)\\
\Theta &= 2\kappa'\theta' + \kappa''\theta - \kappa(k_x^2 + k_z^2)\theta + \kappa\theta'',\\
\frac{\mu}{\mu_2} &= \left(\frac{T}{T_2}\right)^{0.72}, \quad \lambda = -\frac{2}{3}\mu,\\
\nabla\cdot\mathbf{u} &= \mathrm{i}k_x u + v' + \mathrm{i}k_z w, \quad (\cdot)' := \frac{\mathrm{d}(\cdot)}{\mathrm{d}y_w}.
\end{aligned} \tag{7}$$

Here, u, v, and w are the fluctuation velocity components along the x_w, y_w, and z directions, respectively. θ is the perturbation temperature. In symbolic form equations (6) can be rewritten as,

$$\frac{\partial}{\partial t}\mathbf{q} = \boldsymbol{\mathcal{A}}\mathbf{q}, \tag{8}$$

which describes the dynamics of the perturbation field $\mathbf{q} := (u, v, w, \theta)^T$ at given values of the pair (k_x, k_z) denoting the streamwise and spanwise wavenumbers, respectively. In addition to (k_x, k_z), the system in equation (12) is also parametrized by the Reynolds number Re_l which is defined in terms of the flow quantities in the region-2,

$$Re_l = \frac{\rho_2 U_2 l}{\mu_2}, \tag{9}$$

where the length scale $l := \sqrt{x_w\mu_2/(\rho_2 U_2)}$ at x_w streamwise distance from the nose-tip. This definition of Reynolds number can be related to Reynolds number based on the radius $\mathcal{R}$. At a fixed angle φ (see the sketch in figure 1(b) for illustration), we can utilize equations (1) and (9) to obtain

the following relationship,

$$Re_l^2 = \varphi Re_n, \tag{10}$$

where,

$$Re_n = \frac{\rho_2 U_2 \mathcal{R}_n}{\mu_2}. \tag{11}$$

In this paper, we are interested in quantifying the amplification of exogenous disturbances. To accomplish this objective, we augment the evolution model (8) with external excitation sources

$$\begin{aligned} \frac{\partial}{\partial t}\mathbf{q} &= \boldsymbol{\mathcal{A}}\mathbf{q} + \boldsymbol{\mathcal{B}}\mathbf{d} \\ \phi &= \boldsymbol{\mathcal{C}}\mathbf{q} \end{aligned} \tag{12}$$

where, $\mathbf{d} := (d_x, d_y, d_z, d_t)^T$ is a spatially distributed and temporally varying disturbance source (input). For the present study, we assume that $\boldsymbol{\mathcal{B}} = \boldsymbol{\mathcal{C}} = \boldsymbol{\mathcal{I}}$, i.e. the disturbances are allowed to influence the state equation directly and all the state variables are of interest. To characterize the evolution of flow fluctuations described by equation (12), we utilize a finite dimensional approximation by using Chebyshev polynomials [30]. After discretization using, say, N collocation points [30] in the wall-normal direction at a given value of (k_x, k_z), equation (12) can be simplified and rewritten as,

$$\frac{\mathrm{d}}{\mathrm{d}t}\bar{\boldsymbol{\psi}} \;=\; \bar{\boldsymbol{A}}\bar{\boldsymbol{\psi}} + \bar{\mathbf{f}}, \tag{13}$$

where $\bar{\boldsymbol{A}} \in \mathbb{C}^{N\times N}$, $\bar{\boldsymbol{\psi}} \in \mathbb{C}^{N\times 1}$, and $\bar{\mathbf{f}} \in \mathbb{C}^{N\times 1}$ denotes the discretized linear operator $\mathcal{A}$, state $\mathbf{q}$, and the forcing $\mathbf{d}$, respectively.

A. Energy norm for stagnation-point hypersonic flow

We utilize Chu's [31] compressible energy norm to quantify the amplification of flow fluctuations in the presence of external disturbances. The resulting compressible energy density for an ideal gas can be defined as,

$$\|\mathbf{q}\|_E^2 = \int_0^\infty \frac{\rho_2}{2}(u^2+v^2+w^2) + \frac{p_2}{2(\gamma-1)T_2^2}\theta^2 \,\mathrm{d}y_w, \tag{14}$$

where, p_2 denotes the pressure in the region-2 after the shock. Near the stagnation point, p_2 can be well approximated as the stagnation pressure using the following expression,

$$p_2 = \frac{2\gamma}{\gamma+1}M^2 p_1, \tag{15}$$

here, p_1 is the pressure in region-1 before the shock and we have utilized the assumption $M \gg 1$ in region-1. In the non-dimension variables $p_1 = 1/(\gamma M^2)$, leading to the following expression for energy density in the stagnation region,

$$\|\mathbf{q}\|_E^2 = \int_0^\infty \frac{\rho_2}{2}(u^2+v^2+w^2) + \frac{1}{(\gamma^2-1)T_2^2}\theta^2 \,\mathrm{d}y_w. \tag{16}$$

For numerical computations, we choose a finite but large enough length L in the wall-normal direction. With this approximation, the energy norm in equation (16) can be expressed as an inner product,

$$E \;=\; \langle \boldsymbol{\psi}, \boldsymbol{\psi}\rangle_e = \frac{1}{2}\int_0^L \boldsymbol{\psi}^*\mathbf{Q}\boldsymbol{\psi}\mathrm{d}y =: \langle \boldsymbol{\psi}, \mathbf{Q}\boldsymbol{\psi}\rangle, \tag{17}$$

where $\langle\cdot,\cdot\rangle$ denotes the standard L_2 inner product and $\mathbf{Q} := \mathrm{diag}(\rho,\rho,\rho,2/((\gamma^2-1)T_2^2))$ is the energy weighting matrix. After wall-normal discretization, the energy norm is determined by $E = \bar{\boldsymbol{\psi}}^* {I_W}^{1/2}\bar{\mathrm{Q}}{I_W}^{1/2}\bar{\boldsymbol{\psi}} = \bar{\boldsymbol{\psi}}^*\mathrm{Q}\bar{\boldsymbol{\psi}}$, where $\bar{\mathrm{Q}}$ is the finite-dimensional representation of the operator $\mathbf{Q}$ and the I_W is the diagonal matrix of integration weights.

Since the matrix Q is positive-definite, the state of the linearized equation (13) can be transformed into a set of coordinates in which the energy is determined by the standard Euclidean norm, i.e., $E = \boldsymbol{\psi}^*\boldsymbol{\psi}$ with $\boldsymbol{\psi} := \mathrm{Q}^{1/2}\bar{\boldsymbol{\psi}}$. With this change of coordinates, and defining $\boldsymbol{A} := \mathrm{Q}^{1/2}\bar{\mathbf{A}}\mathrm{Q}^{-1/2}$ and $\mathbf{f} := {I_W}^{1/2}\bar{\mathbf{f}}$, we can rewrite the linearized dynamics in equation (13) as,

$$\frac{\mathrm{d}}{\mathrm{d}t}\boldsymbol{\psi} \;=\; \boldsymbol{A}\boldsymbol{\psi} + \mathbf{f}, \tag{18}$$

B. Response to stochastic excitations

Our numerical computations indicate that the linearized dynamical generator $\boldsymbol{A}$ in equation (18) is stable across the range of radii $\mathcal{R}$ and wall temperatures g_w. This observation is consistent with previous studies on hypersonic blunt body flows, which demonstrate that the favorable pressure gradient near the stagnation region stabilizes the classical hydrodynamic instabilities observed in compressible boundary layer flows [8], [13].

In order to model the stochastic sources of uncertainties such as free-stream turbulence encountered in hypersonic wind-tunnels, the external disturbance $\mathbf{f}$ in equation (18) is assumed to be zero-mean and white-in-time stochastic forcing with covariance $\Omega = \Omega^* = I$, i.e.,

$$\mathbb{E}\left(\mathbf{f}\left(t_1\right)\mathbf{f}^*\left(t_2\right)\right) \;=\; I^{4\mathrm{N}\times 4\mathrm{N}}\delta\left(t_1 - t_2\right). \tag{19}$$

Here, $\mathbb{E}(\cdot)$ denotes the expectation operator and * denotes the complex-conjugate-transpose. In the statistical steady state, the covariance matrix at a given wavenumber pair $\mathbf{k} := (k_x, k_z)$,

$$X(\mathbf{k}) = \lim_{t\to\infty}\mathbb{E}\left(\boldsymbol{\psi}(\mathbf{k},t)\boldsymbol{\psi}^*(\mathbf{k},t)\right), \tag{20}$$

is determined by the solution to the Lyapunov equation,

$$A(\mathbf{k})X(\mathbf{k}) + X(\mathbf{k})A^*(\mathbf{k}) = -I. \tag{21}$$

The energy amplification of the stochastically-forced flow can be computed using the solution to equation (21) as:

$$E(\mathbf{k}) \;=\; \mathrm{trace}(X(\mathbf{k})). \tag{22}$$

The above expression for the energy $E(\mathbf{k})$ also represents the $\mathcal{H}_2$-norms of the system (12) at a given (k_x, k_z).

IV. Energy amplification in a hypersonic blunt body flow

In what follows, we will utilize the analysis presented in the previous section to quantify energy amplification in the

TABLE I

FREE-STREAM CONDITIONS FOR BLUNT BODY FLOW

M_∞	T_∞	U_∞	ρ_∞
10	227 K	3000 m/s	0.01 Kg/m^3

presence of external stochastic forcing in a hypersonic blunt body flow.

The dimensional free-stream conditions in the region-1 chosen for the present work are presented in table I. These conditions are typical in flight and we utilize the expressions presented in section II-.1 to obtain the flow in the region-2. Furthermore, we assume a fixed angular location of $\varphi = 5^\circ$ from the stagnation point for all the results presented in this section. The linearized dynamics in the equation (18) are numerically approximated over a domain of height $L = 75$ using 600 Chebyshev collocation points for the state vector ψ (i.e., 150 points for each of the fluctuation quantity). By increasing the number of points it is confirmed that this resolution is high enough. Furthermore, we find that the energy of the steady of state response is insensitive to any further increase in the domain height L.

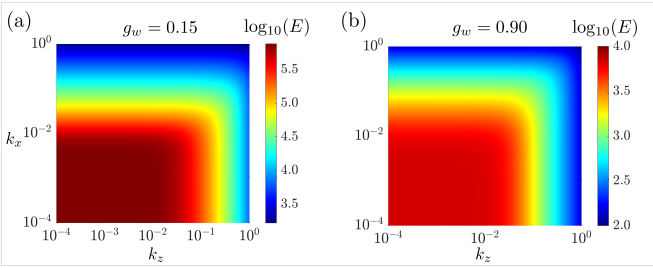

Fig. 2. Plots of $\log_{10}(E(\mathbf{k}))$ in the stagnation point boundary layer subject to white-in-time stochastic excitations at (a) cold wall $g_w = 0.15$ and (b) hot wall $g_w = 0.9$. The Reynolds number based on blunt-body curvature $Re_n = 1.33 \times 10^3$.

Figure 2 shows the energy E associated with the statistical steady state response as a function of the wavenumbers (k_x, k_z) for a flow with a nose-tip Reynolds number $Re_n = 1.33 \times 10^3$ (i.e., a dimensional $\mathcal{R}_n = 1\,\mathrm{cm}$). As shown in the figure, below a certain spanwise and streamwise wavelength, there is a strong attenuation of the energy associated with the flow response. Even though this behavior is independent of the wall temperature, there are some important differences. In particular, in the flow with a colder wall (see figure 2 (a) with $g_w = 0.15$), the fluctuations undergo a much larger amplification than that observed in hotter wall as shown in figure 2 (b) with $g_w = 0.9$.

In addition to the wall-temperature, the radius $\mathcal{R}_n$ acts as an additional parameter which determines the base flow in a blunt body flow. Figure 3 shows the mean flow temperature and velocity profile at a fixed angular location for a range of Reynolds numbers Re_n at a fixed wall temperature $g_w = 0.2$. As the nose-tip becomes more blunt, i.e. as Re_n increases, we observe that the region of high velocity and thermal gradients moves away from the wall. The considerable differences in the mean profile introduced by changing the radius

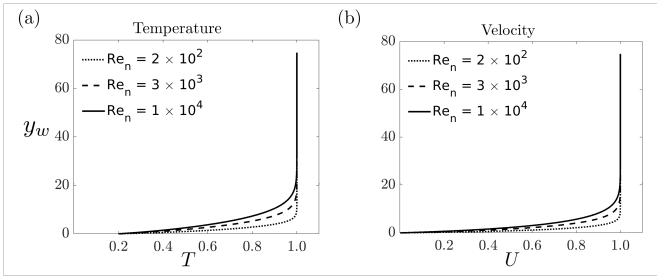

Fig. 3. The wall-normal profile of (a) temperature and (b) velocity for various nose-tip Reynolds number Re_n.

indicate that in addition to wall-temperature, this parameter could play a crucial role in determining amplification of external disturbances.

Figure 4 plots variation of the maximum energy $E_{\max}$ associated with the flow fluctuations that undergo the largest amplification (over k_x, k_z values) for a range of curvature-based Reynolds number Re_n and wall temperature g_w. Figure 4 (a) shows that there is a considerable change in the overall growth of flow fluctuations as we vary Re_n and g_w. In particular, we note that as the wall-temperature increases, there is a significant decline in the fluctuation energy E. On the hand, an increase in the Re_n causes an increase in E regardless of the parameter g_w. These conclusions are in good agreement with flow experiments over blunt bodies in wind tunnels, where an increase in bluntness or a decrease in wall temperature causes the transition to turbulence to appear closer to the nose-tip [3], [4], [6], [7].

To make these observations quantitative figure 4 (b) plots $E_{\max}$ as a function of Re_n. As shown in the figure, over a cold wall, the energy of the fluctuations grows slightly faster than a quadratic function of Re_n (it goes as $\mathcal{O}(Re_n^{2.4})$). On the other hand, at hot-wall conditions, the E exhibits a much smaller growth. At these conditions, we observe two distinct trends: at lower Re_n, the increase in energy is sub-linear, however, as the Reynolds number increases, it starts to approach a quadratic function of Re_n.

V. CONCLUDING REMARKS

The main objective of the present study has been to analyze the steady state response of hypersonic blunt body flows in the presence of background noise using an input-output approach. The starting point of our analysis is a model for the laminar flow near the stagnation point of the blunt body where the high-speed free-stream flow undergoes a rapid deceleration. By utilizing linearized compressible boundary layer equations, we have demonstrated that the background noise can undergo significant amplification over a range of streamwise and spanwise length scales. Furthermore, we have investigated dependence of the steady state response on important physical parameters which are often used to control the behavior of the laminar blunt body flows. Our analysis indicates that in the presence of external stochastic disturbances, a decrease in the wall temperature and an increase in bluntness can significantly deteriorate the

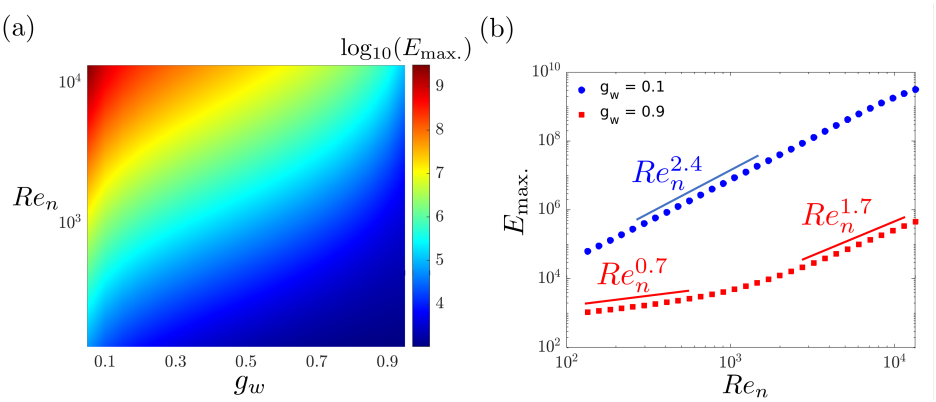

Fig. 4. Plots of maximum energy $\log_{10}(E_{\max.})$ as a function of wall temperature and nose-tip Reynolds number.

robustness of the laminar flow. The point of view adopted in the present work quantifies the influence of uncertainties within an input-output framework and the observations from our analysis are found to agree well with the experimental trends. The present work provides the first steps towards developing control oriented models for flow transition in hypersonic flows. We expect that our work will motivate additional studies for predictive modeling and control of transition to turbulence in high speed flows.

REFERENCES

[1] F. M. White and J. Majdalani, *Viscous fluid flow*. McGraw-Hill New York, 2006, vol. 3.

[2] E. R. Van Driest, *The problem of aerodynamic heating*. Institute of the Aeronautical Sciences, 1956.

[3] R. Dunlap and A. M. Kuethe, "Effects of cooling on boundary-layer transition on a hemisphere in simulated hypersonic flow," *J. Aero. Sc.*, vol. 29, no. 12, pp. 1454–1461, 1962.

[4] K. Stetson, "Nosetip bluntness effects on cone frustum boundary layer transition in hypersonic flow," in *16th Fluid and Plasmadynamics Conference*, 1983, p. 1763.

[5] E. Reshotko, "Transition issues for atmospheric entry," *J. Spacecr. Rockets*, vol. 45, no. 2, pp. 161–164, 2008.

[6] V. Lysenko, "Influence of the entropy layer on the stability of a supersonic shock layer and transition of the laminar boundary layer to turbulence," *J. App. Mech. Tech. Physics*, vol. 31, no. 6, pp. 868–873, 1990.

[7] J. S. Jewell, R. E. Kennedy, S. J. Laurence, and R. L. Kimmel, "Transition on a variable bluntness 7-degree cone at high reynolds number," in *2018 AIAA Aerospace Sciences Meeting*, 2018, p. 1822.

[8] E. Reshotko, "Transient growth: a factor in bypass transition," *Phys. Fluids*, vol. 13, no. 5, pp. 1067–1075, 2001.

[9] P. Paredes, M. M. Choudhari, F. Li, J. S. Jewell, R. L. Kimmel, E. C. Marineau, and G. Grossir, "Nosetip bluntness effects on transition at hypersonic speeds: experimental and numerical analysis under nato sto avt-240," in *2018 AIAA Aerospace Sciences Meeting*, 2018, p. 0057.

[10] L. M. Mack, "Boundary-layer linear stability theory," in *In AGARD, Special Course on Stability and Transition of Laminar Flow*, vol. 1, no. 109, 1984.

[11] L. N. Trefethen, A. E. Trefethen, S. C. Reddy, and T. A. Driscoll, "Hydrodynamic stability without eigenvalues," *Science*, vol. 261, no. 5121, pp. 578–584, 1993.

[12] P. J. Schmid and D. S. Henningson, *Stability and transition in shear flows*. New York: Springer-Verlag, 2001.

[13] E. Reshotko and A. Tumin, "The blunt body paradox—a case for transient growth," in *Laminar-Turbulent Transition*. Springer, 2000, pp. 403–408.

[14] P. Paredes, M. M. Choudhari, and F. Li, "Blunt-body paradox and transient growth on a hypersonic spherical forebody," *Phys. Rev. Fluids*, vol. 2, no. 5, p. 053903, 2017.

[15] S. P. Schneider, "Effects of high-speed tunnel noise on laminar-turbulent transition," *J. Spacecr. Rockets*, vol. 38, no. 3, pp. 323–333, 2001.

[16] S. P. Schneider, "Developing mechanism-based methods for estimating hypersonic boundary-layer transition in flight: The role of quiet tunnels," *Prog. in Aero. Sc.*, vol. 72, pp. 17–29, 2015.

[17] L. Duan, M. M. Choudhari, and C. Zhang, "Pressure fluctuations induced by a hypersonic turbulent boundary layer," *J. Fluid Mech.*, vol. 804, pp. 578–607, 2016.

[18] M. R. Jovanović, "Modeling, analysis, and control of spatially distributed systems," Ph.D. dissertation, University of California, Santa Barbara, 2004.

[19] M. R. Jovanović and B. Bamieh, "Componentwise energy amplification in channel flows," *J. Fluid Mech.*, vol. 534, pp. 145–183, 2005.

[20] M. R. Jovanović, "From bypass transition to flow control and data-driven turbulence modeling: An input-output viewpoint," *Annu. Rev. Fluid Mech.*, vol. 53, no. 1, pp. 311–345, January 2021.

[21] D. Sipp and O. Marquet, "Characterization of noise amplifiers with global singular modes: the case of the leading-edge flat-plate boundary layer," *Theoretical and Computational Fluid Dynamics*, vol. 27, no. 5, pp. 617–635, 2013.

[22] M. Fosas de Pando and P. J. Schmid, "Optimal frequency-response sensitivity of compressible flow over roughness elements," *J. Turbul.*, vol. 18, no. 4, pp. 338–351, 2017.

[23] W. Ran, A. Zare, M. J. P. Hack, and M. R. Jovanović, "Stochastic receptivity analysis of boundary layer flow," *Phys. Rev. Fluids*, vol. 4, no. 9, p. 093901 (28 pages), September 2019.

[24] J. Jeun, J. W. Nichols, and M. R. Jovanović, "Input-output analysis of high-speed axisymmetric isothermal jet noise," *Phys. Fluids*, vol. 28, no. 4, p. 047101 (20 pages), April 2016.

[25] A. Dwivedi, G. S. Sidharth, J. W. Nichols, G. V. Candler, and M. R. Jovanović, "Reattachment vortices in hypersonic compression ramp flow: an input-output analysis," *J. Fluid Mech.*, vol. 880, pp. 113–135, December 2019.

[26] A. Dwivedi, G. S. Sidharth, G. V. Candler, J. W. Nichols, and M. R. Jovanović, "Input-output analysis of shock boundary layer interaction," in *2018 Fluid Dynamics Conference*, 2018, AIAA 2018-3220.

[27] A. Dwivedi, G. V. Candler, and M. R. Jovanović, "A frequency domain analysis of compressible linearized Navier-Stokes equations in a hypersonic compression ramp flow," in *Proceedings of the 2020 American Control Conference*, Denver, CO, 2020, pp. 4325–4330.

[28] A. Dwivedi, G. S. Sidharth, and M. R. Jovanović, "Oblique transition in hypersonic double-wedge flow," *J. Fluid Mech.*, vol. 948, October 2022.

[29] G. V. Candler, H. B. Johnson, I. Nompelis, V. M. Gidzak, P. K. Subbareddy, and M. Barnhardt, "Development of the US3D code for advanced compressible and reacting flow simulations," in *53rd AIAA Aerospace Sciences Meeting*, 2015, aIAA 2015-1893.

[30] J. P. Boyd, *Chebyshev and Fourier spectral methods*. Courier Corporation, 2001.

[31] B.-T. Chu, "On the energy transfer to small disturbances in fluid flow (part i)," *Acta Mech.*, vol. 1, no. 3, pp. 215–234, 1965.